Dynamic component of the asthenosphere: lateral viscosity variations due to dislocation creep at the base of oceanic plates

Vojtěch Patočka[a], Hana Čížková[a] and Jakub Pokorný[a]

[a]Charles University, Faculty of Mathematics and Physics, Department of Geophysics, V Holešovičkách 2, 180 00 Prague, Czech Republic

ARTICLE INFO

Keywords:
Asthenosphere
Dislocation creep
Plate tectonics
Mantle viscosity
Subduction
Numerical modeling

ABSTRACT

The asthenosphere is commonly defined as an upper mantle zone with low velocities and high attenuation of seismic waves, and high electrical conductivity. These observations are usually explained by the presence of partial melt, or by a sharp contrasts in the water content of the upper mantle. Low viscosity asthenosphere is an essential ingredient of functioning plate tectonics. We argue that a substantial component of asthenospheric weakening is dynamic, caused by dislocation creep at the base of tectonic plates. Numerical simulations of subduction show that dynamic weakening scales with the surface velocity both below the subducting and the overriding plate, and that the viscosity decrease reaches up to two orders of magnitude. The resulting scaling law is employed in an apriori estimate of the lateral viscosity variations (LVV) below Earth's oceans. The obtained LVV helps in explaining some of the long-standing as well as recent problems in mantle viscosity inversions.

1. Introduction

Defined as a mechanically weak layer that accommodates vertical isostatic movements of Earth's continents, the asthenosphere is originally a geodynamic concept (Barrell, 1914). Later, it was attributed with low velocities and high attenuation of seismic waves (e.g. Dziewonski and Anderson, 1981; Montagner and Tanimoto, 1991), and also with high electrical conductivity (Shankland et al., 1981) – observations typical for the presence of melt, leading to speculations about widespread partial melting in the upper mantle (e.g. Lambert and Wyllie, 1970; Shankland et al., 1981; Mierdel et al., 2007; Hirschmann, 2010). Recently, Hua et al. (2023) showed that the onset of partial melting is visible in receiver function data from globally distributed seismic stations. Karato (2012), however, argues that the origin of the asthenosphere lies elsewhere. He explains the geophysical observations by assuming a sharp change in the water content of the suboceanic mantle. Due to the second-stage partial melting, ascending mantle material becomes dehydrated approximately 70 km below mid-ocean ridges (Morgan and Morgan, 1999), at the same depth at which the 5-10% drop in seismic velocity is observed in old oceanic plates (e.g. Rychert and Shearer, 2009; Kawakatsu et al., 2009), but where geothermal models predict subsolidus temperatures (i.e., where a sharp contrast in the melt content is unlikely, Fig 5 in Karato, 2012).

A third hypothesis, pursued e.g. by Morgan et al. (2013), is that the asthenosphere is a region where plumes hotter than the average mantle spread below the lithosphere, forming a global pool of elevated temperatures with a negative thermal gradient at its base explaining the gradual increase of seismic velocities at $\sim 250-350$ km depth (Cammarano et al., 2009).

The above three hypotheses of asthenospheric origin are not necessarily contradictory, because they focus on different geophysical observations: i) The lithosphere-asthenosphere boundary (LAB), indicated in the oceanic plates at the depths $\sim$ 70 km by the drop in wavespeed, could be related to a change in the water content, ii) The receiver-function data at $\sim$ 150 km depth (Hua et al., 2023) could be sensitive to a widespread onset of the first-stage, low degree partial melting, iii) The yet deeper increase of seismic velocities at $\sim$ 250 − 350 km depth could be linked with a negative thermal gradient resulting from accumulation of hot material from mantle plumes in the sublithospheric region.

ORCID(s): 0000-0002-3413-6120 (V. Patočka)

Geodynamic significance of the asthenosphere, i.e. that on geological timescales, is in transferring stresses to/from tectonic plates (Forsyth and Uyeda, 1975; Coltice et al., 2019). The lateral extent of some of the major tectonic plates largely exceeds the depth of the mantle, indicating a long-wavelength mantle convection flow (Su and Dziewonski, 1992; Hager and Richards, 1989; Richards and Engebretson, 1992). Such a large aspect ratio cells are, however, theoretically unstable at Earth's Rayleigh number (Busse, 1985; Turcotte and Schubert, 1982) – a viscosity contrast between the asthenosphere and the underlying mantle is required in order to stabilize these long-wavelength structures (Bunge et al., 1996; Ahmed and Lenardic, 2010; Busse et al., 2006; Lenardic et al., 2006).

Lenardic et al. (2019) argue that plate tectonics is a self-sustaining system whose components: the asthenosphere, subducting slabs, and long-wavelength flow are mutually interdependent. Subduction of large tectonic plates generates an asymmetry between the convective velocity of down- and up-flows, which in turn results in a sub-adiabatic thermal gradient in Earth's mantle (Busse, 1985; Jeanloz and Morris, 1987). This, together with the pressure dependence of viscosity, increases the viscosity contrast between the upper and the lower mantle – a necessary ingredient for channelization of horizontal mantle flow and thus for reducing the otherwise destabilizing horizontal drag at the base of large tectonic plates. The system of feedbacks and loops is analyzed in a number of studies (see references in Lenardic et al., 2019) and many of them neglect dislocation creep in the mantle.

All the above studies argue that the asthenosphere is of thermal and/or compositional origin. Here we explore sublithospheric weakening due to dislocation creep at the base of subducting plates, activated by the high strain-rates that result from the relative motion of oceanic plates and the underlying mantle (dynamically generated asthenosphere).

The idea that dislocation creep is important in the shallow mantle is not new. In fact, until the 90s dislocation creep was thought to dominate over diffusion creep throughout the entire upper mantle (e.g. Carter and Ave'Lallemant, 1970; Green and Radcliffe, 1972). Karato and Wu (1993) then argued that dislocation creep is localised only in the asthenosphere while the cold and shallow and the deeper mantle deform via diffusion creep. Dislocation creep is also the main candidate for generating a lattice preferred orientation in minerals and is thus commonly used in interpreting seismic anisotropy, which is strongest near athenospheric depths (e.g. Debayle et al., 2005; Becker et al., 2014; Walpole et al., 2017).

In geodynamic modelling on a regional scale, dislocation creep is also a typical ingredient, promoting strain-rates in regions of high stresses, enhancing velocities (van den Berg et al., 1993) and facilitating motion of the stiff subducting plates (e.g. Billen and Hirth, 2007; Chertova et al., 2012; Yang et al., 2018; Pokorný et al., 2021; Cerpa et al., 2022). Despite these frequent links between dislocation creep and the sublithospheric mantle, the stress-induced (dynamic) contribution of Earth's asthenosphere has not been globally quantified. Dynamic asthenosphere is considered in the works of Semple and Lenardic (2018, 2020, 2021), but their numerical models employ an idealized, layered viscosity structure with activation parameters smaller compared to the experimental values. Moreover, the asthenospheric viscosity reduction is quantified only in the last of these works (Semple and Lenardic, 2021), where a conceptually different, stagnant lid model is investigated, in which weakening is a result of high strain-rates in a convecting layer below an immobile lithosphere (similarly in Schulz et al., 2020).

Mantle viscosity is a key to understanding fundamental Earth science questions and numerous studies attempted to infer it from a wide variety of data. Primary constraints were obtained from the inversions of Earth's geoid (e.g. Hager et al., 1985; Hager and Richards, 1989; Ricard et al., 1993) and postglacial rebound (e.g. Peltier, 1998; Mitrovica and Forte, 2004), and from laboratory experiments of pressurized rocks (e.g. Karato, 2008). Most studies have considered only radially dependent (i.e., 1D) viscosity structure, and yet wide-ranging estimates of viscosity profiles have been obtained. Richards and Lenardic (2018) noted that the mismatch in the astenosphere might be caused by the fact that the long-wavelength geoid and postglacial rebound are both sensitive to a combination of the viscosity contrast between the asthenosphere and underlying mantle and the asthenospheric thickness (Cathles parameter) rather than to the actual value of viscosity in the asthenosphere.

After inversions aiming at the radial viscosity structure, efforts have been invested in inferring also the lateral viscosity variations (LVV) in some parts of the mantle, especially the asthenosphere. Čadek and Fleitout (2003) have demonstrated that the viscosity below the oceanic plates is by 2 orders of magnitude weaker than the deep continental roots. Yang and Gurnis (2016) and Mao and Zhong (2021) assume weak plate margins in their inversions, but do not consider dislocation creep at the base of tectonic plates. Yang and Gurnis (2016) include high-accuracy residual topography measurements into the fitted data and obtain asthenospheric LVV much smaller than those predicted by forward models with laboratory-based activation parameters of diffusion creep – suggesting that some weakening mechanism is missing around the cold and stiff subducting slabs in their models. Mao and Zhong (2021) use weak plate margins in their convection model to obtain surface velocities consistent with the present-day plate motions. In order to match the toroidal component of the surface velocity field, they need to lower the resistance of the circum-pacific plate margin significantly with respect to other plate margins, but a physical reason for such an ad-hoc manipulation is not clear.

Subduction controls the distribution and fragmentation of Earth's tectonic plates (Mallard et al., 2016). Slab dynamics are therefore an important and somewhat independent indicator of the mantle viscosity structure. In the past, subduction models have been used to infer the upper to lower mantle viscosity ratio (Čížková et al., 2012; Liu et al., 2021). Here we estimate the laterally dependent contribution of dislocation creep to sublithospheric weakening, without arguing against thermal and/or compositional effects – the different weakening mechanisms are likely superimposed in the real Earth. We assume that the dynamic weakening stems from the shear of mobile tectonic plates with respect to the underlying mantle. Slab pull on the subducted part of the lithospheric plates drives plate motion which in turn reinforces asthenospheric weakening in a dynamic feedback through nonlinear dislocation creep. We employ numerical models of subduction that include diffusion and dislocation creep with laboratory based parameters (Hirth and Kohlstedt, 2003), and study the relation between plate velocity and asthenospheric weakening. By comparing this relation with the current plate motions, we finally estimate dynamically generated weakening and the resulting lateral viscosity variations (LVV) in the asthenosphere.

2. Subduction models

We perform two families of "generic" subduction models, meaning that the initial and boundary conditions are not tailored to any specific geographic location. The model setup and parameters are similar to those used in previous

studies (Čížková and Bina, 2019) and are listed in Table 1. In one family of models, the overriding plate is attached to the right boundary, mimicking Earth's regions with stationary trench and little to no motion of the overriding plate. In these models, denoted as "fixed OP", the trench rollback does not occur. In the second family of models, labelled as "mobile OP", a mid ocean ridge is imposed at the right top boundary. In this setup OP is free to move trenchwards and thus can accomodate trench rollback. We note that OP is strong and does not allow for horizontal extension, therefore rollback of the SP is associated with the motion of OP as a whole.

Within each family of models, the individual simulations differ by the initial age of the subducting plate, ranging from 50 to 150 Myr at the trench (Table 1). Subduction evolution is evaluated in an extended Boussinesq model that includes buoyancy and latent heat effects of major mantle phase transitions at 410 km and 660 km depths (e.g. Pokorný et al., 2023). A composite rheological model combines diffusion creep, dislocation creep and power-law stress limiter. An effective viscosity of the upper mantle and transition zone is calculated as

$$\eta_{\mathrm{eff}} = \left(\frac{1}{\eta_{\mathrm{diff}}} + \frac{1}{\eta_{\mathrm{disl}}} + \frac{1}{\eta_y} \right)^{-1} . \tag{1}$$

The viscosity of diffusion creep is evaluated as

$$\eta_{\mathrm{diff}} = A_{\mathrm{diff}}^{-1} \exp\left(\frac{E_{\mathrm{diff}} + pV_{\mathrm{diff}}}{RT} \right), \tag{2}$$

where A_{diff} is pre-exponential parameter, E_{diff} is activation energy, p is lithostatic pressure, V_{diff} is activation volume of diffusion creep, R is the gas constant and T is temperature. Dislocation creep viscosity is

$$\eta_{\mathrm{disl}} = A_{\mathrm{disl}}^{-1/n} \, \mathbb{D}_{\|}^{(1-n)/n} \, \exp\left(\frac{E_{\mathrm{disl}} + pV_{\mathrm{disl}}}{nRT} \right), \tag{3}$$

where A_{disl}, E_{disl} and V_{disl} are the pre-exponential parameter, activation energy, and activation volume of dislocation creep, $\mathbb{D}_{\|}$ is the second invariant of the strain rate tensor, and the exponent $n = 3.5$ (Kameyama et al., 1999). Finally the power-law stress limiter viscosity is

$$\eta_y = \sigma_y \mathbb{D}_y{}^{-(1/n_y)} \, \mathbb{D}_{\|}^{(1/n_y)-1} \tag{4}$$

where $\mathbb{D}_y$ is the reference strainrate, σ_y is the yield stress and the power-law exponent is taken as $n_y = 10$.

Activation parameters based on experimental data for wet olivine are assumed in the upper mantle and the transition zone (Hirth and Kohlstedt, 2003). We note that our activation energy of dislocation creep is in the range indicated also by van Hunen et al. (2005) to fit the seismically inferred thermal structure of the Pacific lithosphere. In the lower mantle we assume diffusion creep with parameters based on Čížková et al. (2012). Duration of each simulation is 100 Myr.

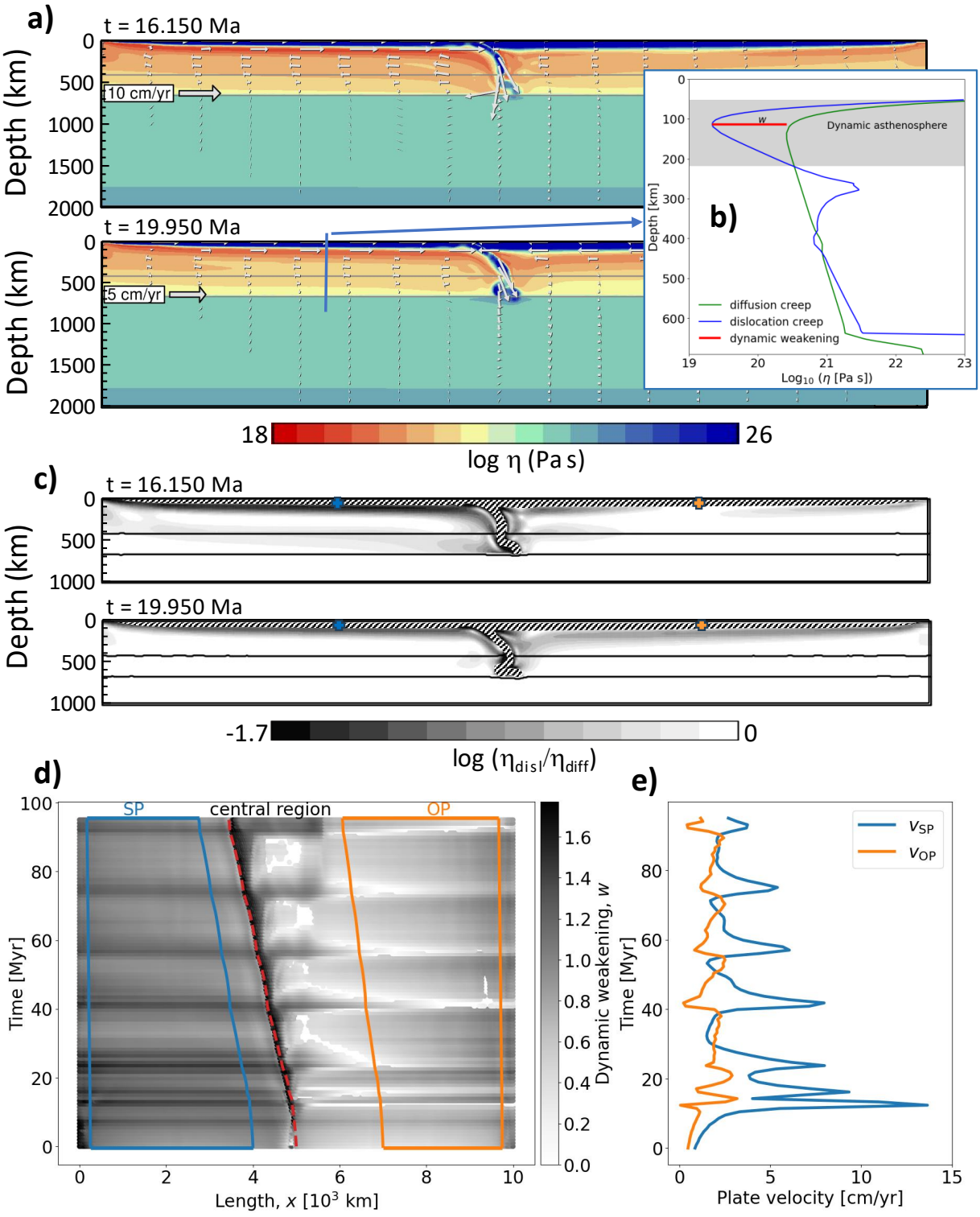

Figure 1: a) Effective viscosity η_{eff} in model M4 (Table 1) for two snapshots in time (t = 16.15 and 19.95 Myr). b) Profile of diffusion and dislocation creep viscosity along a selected vertical line. Dynamic asthenosphere is marked in grey color, the amplitude of dynamic weakening w is marked in red, cf. Eq. (5). c) Ratio of dislocation to diffusion creep viscosity in the upper mantle for the same snapshots as in panel a. Blue and orange crosses depict tracers, placed inside the lithosphere, that are used to evaluate v_{SP} and v_{OP} respectively. Crosshatched regions mark the SP and OP. d) Spatio-temporal evolution of dynamic weakening in model M4. Red dashed line marks the position of the trench, x_{T}, blue and orange lines indicate the length extent over which w is averaged to get $\langle w \rangle$. e) Temporal evolution of subducting (v_{SP}) and overriding (v_{OP}) plate velocities in the same model (M4).

Table 1
Model parameters

Symbol	Meaning	Value	Units
Upper mantle and oceanic lithosphere rheology			
A_{diff}	Pre-exponential parameter of diffusion creep[a]	1×10^{-9}	$Pa^{-1}\ s^{-1}$
A_{disl}	Pre-exponential parameter of dislocation creep[a]	31.5×10^{-18}	$Pa^{-n}\ s^{-1}$
E_{diff}	Activation energy of diffusion creep[a]	3.35×10^{5}	$J\ mol^{-1}$
E_{disl}	Activation energy of dislocation creep[a]	4.8×10^{5}	$J\ mol^{-1}$
V_{diff}	Activation volume of diffusion creep[a]	4.0×10^{-6}	$m^3\ mol^{-1}$
V_{disl}	Activation volume of dislocation creep[a]	11×10^{-6}	$m^3\ mol^{-1}$
n	dislocation creep exponent	3.5	–
$\mathbb{D}_y$	Reference strain rate	1×10^{-15}	s^{-1}
σ_y	Stress limit	2×10^{8}	Pa
n_y	Stress limit exponent	10	–
R	Gas constant	8.314	$J\ K^{-1}\ mol^{-1}$
Lower mantle rheology			
A_{diff}	Pre-exponential parameter of diffusion creep	1.3×10^{-16}	$Pa^{-1}\ s^{-1}$
E_{diff}	Activation energy of diffusion creep[b]	2×10^{5}	$J\ mol^{-1}$
V_{diff}	Activation volume of diffusion creep[b]	1.1×10^{-6}	$m^3\ mol^{-1}$
Other model parameters			
L, D	Model domain dimensions (length, depth)	10^4, $2{\cdot}10^3$	km
κ	Thermal diffusivity	10^{-6}	$m^2\ s^{-1}$
g	Gravitational acceleration	9.8	$m^2\ s^{-2}$
ρ_0	Reference density	3416	$kg\ m^{-3}$
c_p	Specific heat	1250	$J\ kg^{-1}\ K^{-1}$
α_0	Surface thermal expansivity	3×10^{-5}	K^{-1}
γ_{410}	Clapeyron slope of 410 km phase transition[c]	2×10^{6}	$Pa\ K^{-1}$
γ_{660}	Clapeyron slope of 660 km phase transition[c]	-2.5×10^{6}	$Pa\ K^{-1}$
$\delta_{\rho 410}$	Density contrast of 410 km phase transition[d]	273	$kg\ m^{-3}$
$\delta_{\rho 660}$	Density contrast of 660 km phase transition[d]	341	$kg\ m^{-3}$
Description of different models			
Label	Initial age of SP	Initial age of OP	Ridge in the right top corner?
M1	50 Myr	100 Myr	No (fixed OP)
M2	100 Myr	100 Myr	No (fixed OP)
M3	150 Myr	100 Myr	No (fixed OP)
M4	50 Myr	100 Myr	Yes (mobile OP)
M5	100 Myr	100 Myr	Yes (mobile OP)
M6	150 Myr	100 Myr	Yes (mobile OP)
M7	100 Myr	50 Myr	Yes (mobile OP)
M8	100 Myr	150 Myr	Yes (mobile OP)
M9	150 Myr	150 Myr	Yes (mobile OP)

[a] Parameters of wet olivine based on Hirth and Kohlstedt (2003)
[b] Čížková et al. (2012)
[c] Bina and Helffrich (1994)
[d] Steinbach and Yuen (1995)

3. Dynamic weakening below the subducting and overriding plates

In both model families, a distinct region forms below the subducting plate (SP), where the viscosity of dislocation creep is smaller than that of diffusion creep. We denote this compact, sub-plate domain where $\eta_{\mathrm{disl}} < \eta_{\mathrm{diff}}$ as the "dynamic asthenosphere" (or simply the asthenosphere in the following text). We define the dynamic weakening w as

$$w\,(x,t) = \log \frac{\min\,(\eta_{\mathrm{disl}})}{\min\,(\eta_{\mathrm{diff}})}, \tag{5}$$

(cf. also Fig. 1b). The quantity w is a measure of the viscosity reduction that is caused by the high strain-rate below the plate (or by the high stress – note that dislocation creep viscosity can be formulated either as a function of strain-rate or as a function of stress (van den Berg et al., 1993)). At each time t for each horizontal position x, the minima in Eq. (5) are found over the entire domain depth. In Fig. 1d, we show how w is distributed both horizontally and temporarily in model M4.

The value of w is approximately constant up to $x \approx 0.8\,x_{\mathrm{T}}$, where x_{T} is the (time varying) position of the trench. In subsequent analysis, we will represent the dynamic weakening below the SP with the value of w averaged over $x \in (0.05,\ 0.8)\,x_{\mathrm{T}}$ to avoid regions near the plate boundaries (ridge and trench) which are dominated by vertical flow (discussion of the near-trench region follows at the end of this section).

As the subducting slab starts sinking into the mantle, its velocity v_{SP} varies due to the increasing slab pull, varying resistance of the mantle and petrological buoyancy associated with the phase transitions (Fig. 1e). First, the plate speeds up as the 410 km phase transition enhances the slab pull, then it slows down in response to the 660 km phase transition and to the viscosity increase in the lower mantle. In later stages, variations of plate velocity are driven by slab buckling (Čížková and Bina, 2013).

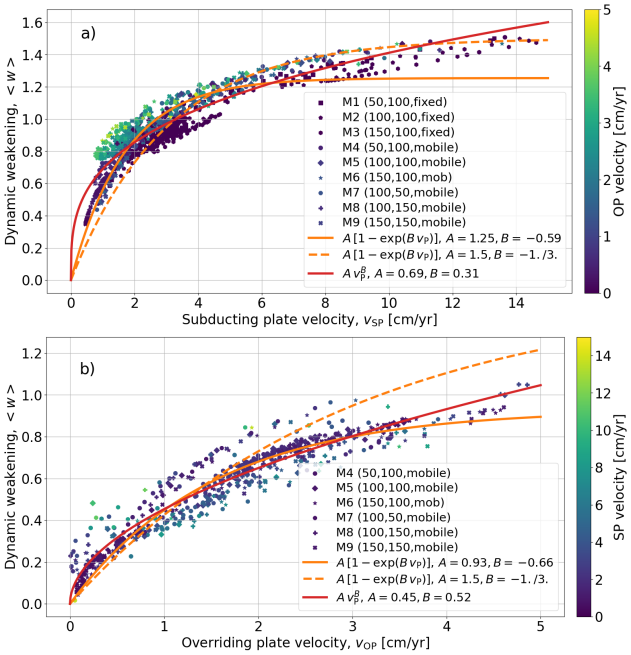

Figure 2: a) Dynamic weakening w below the SP, averaged over the segment $x \in (0.05x_{\mathrm{T}},\ 0.8x_{\mathrm{T}})$ (cf. the blue segment in Fig. 1d), plotted as a function of the SP velocity v_{SP}. Different symbols represent different models (Table 1), color marks the OP velocity v_{OP} in each respective snapshot in time. Orange curve shows the best fit of the data using Eq. (6), dashed line is the parametrization that we employ in Fig. 3. b) Dynamic weakening below the OP (orange segment in Fig. 1d). Color marks the SP velocity v_{SP}.

We assume that the magnitude of strain-rate in the asthenosphere is primarily controlled by the contrast of plate velocity with respect to the underlying mantle and therefore aim to derive a relation between dynamic weakening and plate velocity. Fig. 2a shows that the plate velocity v_{SP} provides a primary control on the dynamic weakening below the SP, because the same trend is observed for all the models, i.e. regardless of the initial plate age. The data indicate first a steep increase of $<w>$ with v_{SP}, and then the slope decreases when plate velocity is higher. We choose a two parameter fit using an exponential function,

$$f(v_{\mathrm{P}}) = A \cdot \left(1 - \exp\left(B \cdot v_{\mathrm{P}}\right)\right) \tag{6}$$

where v_P is the plate velocity in cm/yr ($v_P = v_{SP}$ in Fig. 2a and $v_P = v_{OP}$ in Fig. 2b). Simultaneous fit of the data from all the performed simulations gives $A = 1.25$ and $B = 0.59$ below SP, root mean square error of the fit is 0.09.

In the family of fixed OP models, dynamic weakening is measured only below the SP. In mobile OP models, a similar effect is observed and measured also below the overriding plate. In Fig. 2b, we plot $<w>$ evaluated below the OP as a function of the rollback velocity, v_{OP}. The weakening below OP is represented by an average value of w over the segment $(x - x_T)/(L - x_T) \in (0.4, 0.95)$, with L denoting the length of the model, $L = 10^4$ km (see the orange segment in Fig. 1d).

Similarly to SP (Fig. 2), also under OP the dependence of dynamic weakening on the plate velocity is comparable in all the investigated models, implying that the $<w>(v_P)$ scaling law, Eq. (6), is applicable to a generic subduction setting. The dynamic weakening is, however, less spatially uniform below OP when compared to SP (see Fig. 1d), with w slightly increasing toward the right edge, making the average value $<w>$ somewhat dependent on the x-range over which the average is computed. Nevertheless, in first approximation, the asthenosphere below OP can be represented with the same $<w>(v_P)$ relationship as the asthenosphere below SP (cf. the orange dashed line in Fig. 2).

The color of symbols in Fig. 2 marks the complementary plate velocity. Fig. 2a shows that dynamic weakening below SP is enhanced when OP velocity is high, while dynamic weakening below OP seems to be slightly reduced for most data points with a high v_{SP}, with the exception of when OP is nearly stagnant ($v_{OP} < 1$ cm/yr). This behaviour is related to the interplay between the two plates during buckling.

The subducting plate velocity, v_{SP}, undergoes quasi-periodic variations (described in more detail in e.g. Čížková and Bina (2013)). In the episodes of fast v_{SP} when the dip angle of the slab increases, there is a negligible rollback and OP is more less stagnant. Below SP is a return flow (Fig. 1a) whose strength, and thus the amplitude of dynamic weakening, is governed entirely by v_{SP} at this stage of subduction. Weakening of the mantle wedge is also dominated by v_{SP} during this stage, because the fast-sinking slab weakens the mantle at its base and above its upper surface. The overriding plate velocity, v_{OP} is typically small when v_{SP} is large, and dynamic weakening below OP is also small (Fig. 1d).

In a complementary stage, typically when a large segment of the slab encounters an increased resistance at the 660 km phase transition, v_{SP} decreases and low dip angle results in a fast rollback episode accompanied by an increase of the rollback velocity (Fig. 1e). The strength of return flow below SP is partly governed by how fast the SP is 'laying flat', which is, however, related to the rollback velocity, v_{OP}. This explains why the data points in Fig. 2a that correspond to time steps with a high v_{OP} (bright color) show above average weakening. At this stage, v_{OP} is relatively large, and the mantle wedge is dominated by the flow below the OP, which has the same direction as that of the plate and magnitude decreasing with depth (Couette flow).

As a result, dynamic weakening above the already flat-lying slab shows a more complicated pattern and is cyclically governed by either v_{SP} or v_{OP}. This is a natural consequence of the fact that the central region (Fig. 1d) progressively contains both the SP and OP, which disrupts the simple relation between asthenospheric viscosity and the surface velocity described by Eq. (6). We exclude the central region from the analysis in Fig. 2.

Nevertheless, Eq. (6) provides a reasonable first-order estimate for the global distribution of the dynamic weakening w. In the next section, we apply the formula $w = 1.5\,[1-\exp(-v_\mathrm{P}/3)]$ to estimate LVV below Earth's oceans.

Both below the SP and OP, the dynamic asthenosphere has an average central depth of ca. 150 km, and is ca. 200 km thick (cf. the grey area in Fig. 1b), which agrees with the common definition of asthenosphere that is based on seismic and electromagnetic sounding observations.

4. Dynamic LVV

Inferring mantle viscosity from geophysical observations is a tedious but important task. The available data are insufficient to perform a 3D inversion without making additional simplifying assumptions (e.g. Čadek and Fleitout, 2003). One way to move forward is to improve our apriori knowledge of LVV in the mantle. In this section, we use the empirical law, Eq. (6), to make a first-order estimate of LVV in the asthenosphere from reconstructed values of the absolute surface plate motions (Müller et al., 2019) (Fig. 3).

Using Eq. (6) globally is based on two simplifying assumptions. First, we assume that subduction dynamics dominates asthenospheric flow below the oceans. Coltice et al. (2019) evaluated the areal fraction F_D of the surface that is dragged by the interior in global mantle convection models with imposed continents. The average value of F_D was about 35% in their simulations, with the continental areas contributing to F_D proportionally more than the oceans. Their results imply that the surface plates are the main driver of the interior in oceanic regions, consistently with our approach. Second, we apply Eq. (6) to the entire area of oceanic plates, while the central and ridge regions were excluded from the analysis in Fig. 2 (cf. Fig. 1d).

Despite these crude simplifications, the dynamic LVV predicted in Fig. 3 naturally explain several observations and help in resolving some problems experienced in previously published viscosity inversions. First of all, the dynamic weakening below the oceans is likely to be significantly larger than below the continents. While we restrict our analysis to oceans only, it can be expected that dynamic weakening below the continents is much smaller, because the drift of continents is on average much slower than the average velocity of oceanic plates (e.g. Torsvik et al., 2008). This result is in line with the findings of Ricard et al. (1991) and Čadek and Ricard (1992), who analyze the net rotation of the lithosphere (degree one toroidal velocities) and conclude that "asthenospheric viscosity below the oceans is at least one order of magnitude lower than underneath the continents", consistently with later geoid inversions (Čadek and Fleitout, 2003).

Secondly, the pacific plate is moving fast and thus is most lubricated. In order to match the present-day global surface velocities, Mao and Zhong (2021) had to reduce the resistance of the circum-pacific plate margin by a factor of ca. 7 with respect to other plate margins. However, if the asthenospheric LVV as predicted in Fig. 3 were accounted for in their study, such an ad hoc reduction would not be necessary – the surface velocities of the pacific plate would increase even if the resistance of the circum-pacific plate margin was the same as the resistance of other plate margins. There are two dominant mechanisms that control the surface velocity of a plate: the resistance at its margin, and the friction at its base. The horizontal drag at the base of the pacific plate is significantly smaller than in most other regions (Fig. 3), which may allow for its relatively large surface velocity without the circum-pacific margin's resistance being smaller when compared to other plate margins.

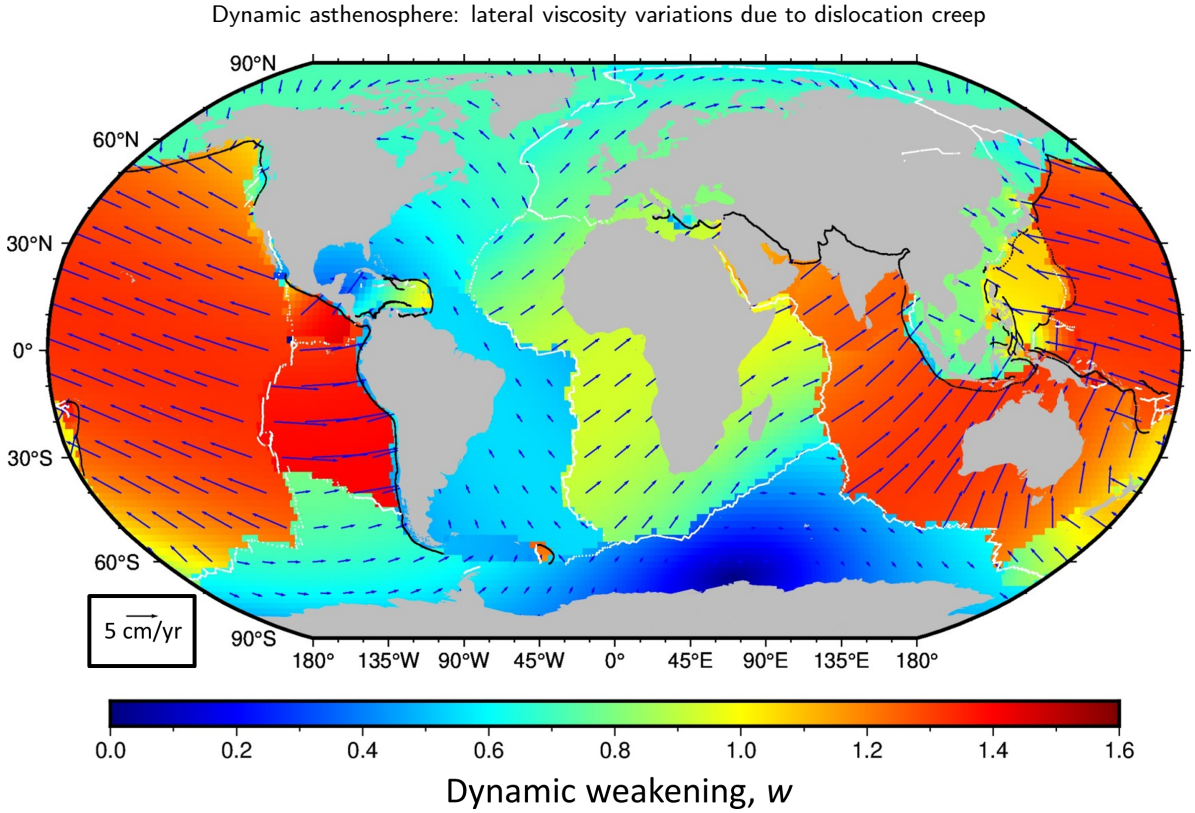

Figure 3: Dynamic weakening below Earth's oceanic plates. Vectors show the absolute plate velocities derived by Müller et al. (2019), obtained with a freely available software package GPlates (Boyden et al., 2011). Sublithospheric dynamic weakening, w, showed in color, is computed from these velocities using our empirical law, $w = 1.5\,[1 - \exp(-v_\mathrm{P}/3)]$. The quantity w represents a first-order estimate of the LVV in the asthenosphere. Grey areas depict Earth's continents, black and white lines show the major trenches and ridges, respectively (Coffin, 1998).

Note also that the surface plate velocities by Müller et al. (2019) are computed such as to minimize the net lithospheric rotation. In reference frames that allow for faster net rotation rates, the westward velocities of plates increase (Doglioni et al., 2015). In this regard, the speed of the Pacific plate in Fig. 3 is the bottom estimate.

Finally, the oldest and thus coldest slabs sink at the fastest rates. Our results therefore suggest that, at large wavelengths, the viscosity variations resulting from temperature effects should be partly compensated by the dynamic weakening. This is in line with the fact that the inverted long-wavelength LVV (e.g. Yang and Gurnis, 2016) are much smaller than those predicted by forward models using laboratory-based constitutive relations for diffusion creep, in which the variations are suggested to be at least several orders of magnitude (e.g. Stadler et al., 2010).

5. Discussion and conclusions

We have evaluated the sublithospheric viscosity of dislocation and diffusion creep in a number of free subduction simulations. There is a significant dynamic weakening below both the subducting and the overriding plate, and it is primarily controlled by the amplitude of the surface velocity.

Given the importance of asthenosphere in the plate tectonics theory, our results warn against the use of numerical simulations with only diffusion creep. In a series of papers summarized by Lenardic et al. (2019), the viscosity contrast between the asthenosphere and the underlying mantle is linked with a sub-adiabatic temperature profile that results from an asymmetry between up- and down-wellings. Here, we show that a significant viscosity contrast may result simply from the relative motion of tectonic plates with respect to the underlying mantle.

The mutual feedback between plate velocities and their basal lubrication is likely to play a role during tectonic history of Earth. A drawback of the exponential law, Eq.(6), is its quick saturation, resulting in an underestimation of dynamic weakening when plate velocities are higher than ca. 20 cm/yr (based on additional simulations not shown here). In order to predict dynamic weakening in episodes of rapid plate motions, that is, for a broader range of v_P, we find that power-law is more suitable ($<w> = A\, v_\mathrm{P}^B$ gives a comparable fit also in the here studied range of v_P, see the red solid line in Fig. 2).

The volume fraction of partial melt is likely less than 0.1% away from mid ocean ridges (e.g. Karato, 2012), and the presence of the 150-km (i.e. the first-stage melting) boundary showed no correlation with radial seismic anisotropy, indicating that partial melt has no substantial effect on the large-scale viscosity of the asthenosphere (Hua et al., 2023). Increased water content or elevated temperatures due to the accumulation of plume material are, however, likely to produce additional, significant LVV in Earth's upper mantle. It is important to stress that we do not argue against the presence of partial melt, variations in the water content, or pooling of plume material in Earth's upper mantle.

The presence or absence of asthenosphere is often debated in the context of Venus (e.g. Pauer et al., 2006). Recently, Maia et al. (2023) performed a global inversion of Venus's geoid and topography using a Bayesian inference approach. They inferred a $\sim$ 235 km thin, low-viscosity zone with a viscosity reduction of 5–15 times with respect to the underlying mantle. Given the different tectonic regime of Earth and Venus, a less pronounced asthenosphere on Venus is consistent with dynamic weakening being a significant, but not the sole mechanism involved.

There is a notable difference between the sublithospheric flow structure in our models when compared to typical global models (e.g. Lenardic et al., 2019; Coltice et al., 2019). While in the global models, Couette or Poiseuille flow dominates below the oceanic plates (i.e. plates drag the interior or the interior drags the surface plates), in our simulations, which contain more realistic slab dynamics, the sublithospheric mantle is driven by the return flow below the sinking slab (Fig. 1a, the return flow is confined in the upper mantle). In this particular aspect, our simulations are similar to those presented by Morgan et al. (2013), who show that bulk of the asthenosphere resists being dragged down at the subduction zone (cf. their Fig. 1 and Section 2.3). They argue that grid resolution of 4 km is needed to capture this behaviour, far less than in typical global simulations. Note, however, that when slab penetrates into the lower mantle, which happens in models with fixed overriding plate, a whole-mantle convection cell develops below the SP. In our case, the return flow in the upper mantle is thus related to the folding of the slab in the transition zone rather than to the return of anomalously hot material as in Morgan et al. (2013). Note also that Fig. 2a contains data from all our simulations over the entire simulation time (100 Myr), indicating that the scaling law in Eq. (6) captures the behaviour both before and after the penetration of the slab into the lower mantle.

On the other hand, regional modelling suffers from the intrinsic incapability to capture how local dynamics affect the global flow structure, which in turn determines the boundary conditions of regional-scale models. To fully reconcile the above discrepancy, one must perform global numerical simulations with grid resolution of present-day regional models – a challenging task. In one case or the other, strain rates are likely to be high below the fast moving

tectonic plates, and we show that dynamic weakening due to dislocation creep is an important mechanism under such conditions, significantly contributing to the formation of the low-viscosity asthenosphere.

6. Acknowledgements

We thank Arie van den Berg for discussions on the nolinear rheology of upper mantle and Wim Spakman for sharing his script for viscosity/velocity plots. This work has been supported by Charles University Research Centre program No. UNCE/24/SCI/005.

Open Research

The viscosity fields, interpolated onto a regular grid, and the time evolution of plate velocities in all models, as well as scripts that were used to produce Fig. 1b,c,d,e and Fig. 2 are available at Zenodo (Patočka, 2024). Figure 1a was produced using the python interface for the Generic Mapping Tool (pyGMT) software (https://pypi.org/search/?q=pygmt).

CRediT authorship contribution statement

Vojtěch Patočka: Conceptualization, Methodology, Investigation, Visualization, Writing - Original draft preparation. **Hana Čížková:** Conceptualization, Investigation, Visualization, Writing - Review & Editing. **Jakub Pokorný:** Investigation, Visualization, Writing - Review & Editing.

References

Ahmed, O., Lenardic, A., 2010. Low viscosity channels and the stability of long wavelength convection. Phys. Earth Planet. Inter. 179, 122–126. doi:10.1016/j.pepi.2010.01.008.

Barrell, J., 1914. The strength of the earth's crust. The Journal of Geology 22, 655–683. doi:10.1086/622181.

Becker, T.W., Conrad, C.P., Schaeffer, A.J., Lebedev, S., 2014. Origin of azimuthal seismic anisotropy in oceanic plates and mantle. Earth Planet. Sci. Lett. 401, 236–250. doi:10.1016/j.epsl.2014.06.014.

van den Berg, A., van Keken, P., Yuen, D., 1993. The effects of a composite non-newtonian and newtonian rheology on mantle convection. Geophys. J. Int. , 62–78.

Billen, M., Hirth, G., 2007. Rheologic controls on slab dynamics. Geochem. Geophys. Geosyst. 8, Q08012. doi:10.1029/2007GC001597.

Bina, C.R., Helffrich, G., 1994. Phase transition Clapeyron slopes and transition zone seismic discontinuity topography. Journal of Geophysical Research: Solid Earth 99, 15853–15860. doi:10.1029/94JB00462.

Boyden, J.A., Müller, R.D., Gurnis, M., Torsvik, T.H., Clark, J.A., Turner, M., Ivey-Law, H., Watson, R.J., Cannon, J.S., 2011. Next-generation plate-tectonic reconstructions using gplates .

Bunge, H., Richards, M., Baumgardner, J., 1996. Effect of depth-dependent viscosity on the planform of mantle convection. Nature 379, 436–438. doi:10.1038/379436a0.

Busse, F., Richards, A., Lenardic, A., 2006. A simple model of high prandtl and high rayleigh number convection bounded by thin low-viscosity layers. Geophys. J. Int. 164, 160–167. doi:10.1111/j.1365-246X.2005.02836.x.

Busse, F.H., 1985. Transition to turbulence in Rayleigh-Beénard convection. Springer Berlin Heidelberg, Berlin, Heidelberg. pp. 97–137. URL: https://doi.org/10.1007/3-540-13319-4_15, doi:10.1007/3-540-13319-4_15.

Cammarano, F., Romanowicz, B., Stixrude, L., Lithgow-Bertelloni, C., Xu, W., 2009. Inferring the thermochemical structure of the upper mantle from seismic data. Geophys. J. Int. 179, 1169–1185. doi:10.1111/j.1365-246X.2009.04338.x.

Carter, N., Ave'Lallemant, H., 1970. High Temperature Flow of Dunite and Peridotite. GSA Bulletin 81, 2181–2202. doi:10.1130/0016-7606(1970)81[2181:HTFODA]2.0.CO;2.

Cerpa, N.G., Sigloch, K., Garel, F., Heuret, A., Davies, Rhodri, D., Mihalynuk, M.G., 2022. The effect of a weak asthenospheric layer on surface kinematics, subduction dynamics and slab morphology in the lower mantle. J. Geophys. Res. , e2022JB024494doi:10.1029/2022JB024494.

Chertova, M., Geenen, T., van den Berg, A., Spakman, W., 2012. Using open sidewalls for modelling self-consistent lithosphere subduction dynamics. Solid Earth , 313–326doi:10.5194/se-3-313-2012.

Coffin, M., 1998. Present-day plate boundary digital data compilation. University of Texas Institute for geophysics technical report 174, 5.

Coltice, N., Husson, L., Faccenna, C., Arnould, M., 2019. What drives tectonic plates? Sci. Advances 5. doi:10.1126/sciadv.aax4295.

Debayle, E., Kennett, B., Priestley, K., 2005. Global azimuthal seismic anisotropy and the unique plate-motion deformation of australia. NATURE 433, 509–512. doi:10.1038/nature03247.

Doglioni, C., Carminati, E., Crespi, M., Cuffaro, M., Penati, M., Riguzzi, F., 2015. Tectonically asymmetric earth: From net rotation to polarized westward drift of the lithosphere. Geoscience Frontiers 6, 401–418. doi:10.1016/j.gsf.2014.02.001.

Dziewonski, A., Anderson, D., 1981. Preliminary reference earth model. Phys. Earth Planet. Inter. 25, 297–356. doi:10.1016/0031-9201(81)90046-7.

Forsyth, D., Uyeda, S., 1975. Relative importance of driving forces of plate motion. Geophys. J. Royal Astro. Soc. 43, 163–200. doi:10.1111/j.1365-246X.1975.tb00631.x.

Green, H., Radcliffe, S., 1972. Dislocation mechanisms in olivine and flow in the upper mantle. Earth Planet. Sci. Lett. 15, 239–247. doi:10.1016/0012-821X(72)90169-0.

Hager, B., Clayton, R., Richards, M., Comer, R., Dziewonski, A., 1985. Lower mantle heterogeneity, dynamic topography and the geoid. Nature 313, 541–546. doi:10.1038/313541a0.

Hager, B., Richards, M., 1989. Long-wavelength variations in earth's geoid - physical models and dynamical implications. Philos. Trans. R. Soc. London 328, 309–327. doi:10.1098/rsta.1989.0038.

Hirschmann, M.M., 2010. Partial melt in the oceanic low velocity zone. Phys. Earth Planet. Inter. 179, 60–71. doi:10.1016/j.pepi.2009.12.003.

Hirth, G., Kohlstedt, D., 2003. Rheology of the upper mantle and the mantle wedge: A view from the experimentalists. Inside the subduction factory, Geophysical monograph 138 doi:10.1029/138GM06.

Hua, J., Fischer, K.M., Becker, T.W., Gazel, E., Hirth, G., 2023. Asthenospheric low-velocity zone consistent with globally prevalent partial melting. Nat. Geo doi:10.1038/s41561-022-01116-9.

van Hunen, J., Zhong, S., Shapiro, N.M., Ritzwoller, M.H., 2005. New evidence for dislocation creep from 3-d geodynamic modeling of the pacific upper mantle structure. Earth Planet. Sci. Lett. , 146–155doi:10.1016/j.epsl.2005.07.006.

Jeanloz, R., Morris, S., 1987. Is the mantle geotherm subadiabatic. Geophys. Res. Let. 14, 335–338. doi:10.1029/GL014i004p00335.

Kameyama, M., Yuen, D., Karato, S., 1999. Thermal-mechanical effects of lowtemperature plasticity (the peierls mechanism) on the deformation of a viscoelastic shear zone. Earth Planet. Sci. Lett. , 159–172.

Karato, S., Wu, P., 1993. Rheology of the upper mantle - a synthesis. Science 260, 771–778. doi:10.1126/science.260.5109.771.

Karato, S.i., 2008. Insights into the nature of plume-asthenosphere interaction from central pacific geophysical anomalies. Earth Planet. Sci. Lett. 274, 234–240. doi:10.1016/j.epsl.2008.07.033.

Karato, S.i., 2012. On the origin of the asthenosphere. Earth Planet. Sci. Lett. 321, 95–103. doi:10.1016/j.epsl.2012.01.001.

Kawakatsu, H., Kumar, P., Takei, Y., Shinohara, M., Kanazawa, T., Araki, E., Suyehiro, K., 2009. Seismic evidence for sharp lithosphere-asthenosphere boundaries of oceanic plates. SCIENCE 324, 499–502. doi:10.1126/science.1169499.

Lambert, I., Wyllie, P., 1970. Low-velocity zone of earths mantle - incipient melting caused by water. Science 169, 764+. doi:10.1126/science.169.3947.764.

Lenardic, A., Richards, M.A., Busse, F.H., 2006. Depth-dependent rheology and the horizontal length scale of mantle convection. J. Geophys. Res. Sol. Earth 111. doi:10.1029/2005JB003639.

Lenardic, A., Weller, M., Hoink, T., Seales, J., 2019. Toward a boot strap hypothesis of plate tectonics: Feedbacks between plates, the asthenosphere, and the wavelength of mantle convection. Phys. Earth Planet. Inter. 296. doi:10.1016/j.pepi.2019.106299.

Liu, H., Gurnis, M., Leng, W., 2021. Constraints on mantle viscosity from slab dynamics. J. Geophys. Res. Sol. Earth 126. doi:10.1029/2021JB022329.

Maia, J.S., Wieczorek, M.A., Plesa, A.C., 2023. The mantle viscosity structure of venus. Geophys. Res. Let. 50, e2023GL103847. doi:10.1029/2023GL103847.

Mallard, C., Coltice, N., Seton, M., Muller, R.D., Tackley, P.J., 2016. Subduction controls the distribution and fragmentation of earth's tectonic plates. Nature 535, 140+. doi:10.1038/nature17992.

Mao, W., Zhong, S., 2021. Constraints on mantle viscosity from intermediate-wavelength geoid anomalies in mantle convection models with plate motion history. J. Geophys. Res. Sol. Earth 126. doi:10.1029/2020JB021561.

Mierdel, K., Keppler, H., Smyth, J.R., Langenhorst, F., 2007. Water solubility in aluminous orthopyroxene and the origin of earth's asthenosphere. Science 315, 364–368. doi:10.1126/science.1135422.

Mitrovica, J., Forte, A., 2004. A new inference of mantle viscosity based upon joint inversion of convection and glacial isostatic adjustment data. Earth Planet. Sci. Lett. 225, 177–189. doi:10.1016/j.epsl.2004.06.005.

Montagner, J., Tanimoto, T., 1991. Global upper mantle tomography of seismic velocities and anisotropies. J. Geophys. Res. Sol. Earth 96, 20337–20351. doi:10.1029/91JB01890.

Morgan, J., Morgan, W., 1999. Two-stage melting and the geochemical evolution of the mantle: a recipe for mantle plum-pudding. Earth Planet. Sci. Lett. 170, 215–239.

Morgan, J.P., Hasenclever, J., Shi, C., 2013. New observational and experimental evidence for a plume-fed asthenosphere boundary layer in mantle convection. Earth Planet. Sci. Lett. 366, 99–111. doi:10.1016/j.epsl.2013.02.001.

Müller, R.D., Zahirovic, S., Williams, S.E., Cannon, J., Seton, M., Bower, D.J., Tetley, M.G., Heine, C., Le Breton, E., Liu, S., Russell, S.H.J., Yang, T., Leonard, J., Gurnis, M., 2019. A global plate model including lithospheric deformation along major rifts and orogens since the triassic. Tectonics 38, 1884–1907. doi:10.1029/2018TC005462.

Patočka, V., 2024. Simulation data for manuscript Dynamic component of the asthenosphere: lateral viscosity variations due to dislocation creep at the base of oceanic plates. doi:10.5281/zenodo.10499016.

Pauer, M., Fleming, K., Cadek, O., 2006. Modeling the dynamic component of the geoid and topography of venus. J. Geophys. Res. Planets 111. doi:10.1029/2005JE002511.

Peltier, W., 1998. Postglacial variations in the level of the sea: Implications for climate dynamics and solid-earth geophysics. Rev. Geophys. 36, 603–689. doi:10.1029/98RG02638.

Pokorný, J., Čížková, H., Bina, C., van den Berg, A., 2023. 2d stress rotation in the tonga subduction region. Earth Planet. Sci. Lett. , 118379doi:10.1016/j.epsl.2023.118379.

Pokorný, J., Čížková, H., van den Berg, A., 2021. Feedbacks between subduction dynamics and slab deformation: Combined effects of non-linear rheology of a weak decoupling layer and phase transitions. Phys. Earth Planet. Inter. doi:10.1016/j.pepi.2021.106679.

Ricard, Y., Doglioni, C., Sabadini, R., 1991. Differential rotation between lithosphere and mantle - a consequence of lateral mantle viscosity variations. J. Geophys. Res. 96, 8407–8415. doi:10.1029/91JB00204.

Ricard, Y., Richards, M., Lithgow-Bertelloni, C., Lestunff, Y., 1993. A geodynamic model of mantle density heterogeneity. J. Geophys. Res. Sol. Earth 98, 21895–21909. doi:10.1029/93JB02216.

Richards, M., Engebretson, D., 1992. Large-scale mantle convection and the history of subduction. Nature 355, 437–440. doi:10.1038/355437a0.

Richards, M.A., Lenardic, A., 2018. The cathles parameter (ct): A geodynamic definition of the asthenosphere and implications for the nature of plate tectonics. Geochem. Geophys. Geosyst. 19, 4858–4875. doi:10.1029/2018GC007664.

Rychert, C.A., Shearer, P.M., 2009. A global view of the lithosphere-asthenosphere boundary. Science 324, 495–498. doi:10.1126/science.1169754.

Schulz, F., Tosi, N., Plesa, A.C., Breuer, D., 2020. Stagnant-lid convection with diffusion and dislocation creep rheology: Influence of a non-evolving grain size. Geophys. J. Int. 220, 18–36. doi:10.1093/gji/ggz417.

Semple, A., Lenardic, A., 2020. The robustness of pressure-driven asthenospheric flow in mantle convection models with plate-like behavior. Geophys. Res. Let. 47. doi:10.1029/2020GL089556.

Semple, A.G., Lenardic, A., 2018. Plug flow in the earth's asthenosphere. Earth Planet. Sci. Lett. 496, 29–36. doi:10.1016/j.epsl.2018.05.030.

Semple, A.G., Lenardic, A., 2021. Feedbacks between a non-newtonian upper mantle, mantle viscosity structure and mantle dynamics. Geophys. J. Int. 224, 961–972. doi:10.1093/gji/ggaa495.

Shankland, T., O'Connell, R., Waff, H., 1981. Geophysical constraints on partial melt in the upper mantle. Rev. Geophys. 19, 394–406. doi:10.1029/RG019i003p00394.

Stadler, G., Gurnis, M., Burstedde, C., Wilcox, L.C., Alisic, L., Ghattas, O., 2010. The dynamics of plate tectonics and mantle flow: From local to global scales. Science 329, 1033–1038. doi:10.1126/science.1191223.

Steinbach, V., Yuen, D.A., 1995. The effects of temperature-dependent viscosity on mantle convection with the two major phase transitions. Physics of the Earth and Planetary Interiors 90, 13 – 36. doi:10.1016/0031-9201(95)03018-R.

Su, W., Dziewonski, A., 1992. On the scale of mantle heterogeneity. Phys. Earth Planet. Inter. 74, 29–54. doi:10.1016/0031-9201(92)90066-5.

Torsvik, T.H., Müller, R.D., Van der Voo, R., Steinberger, B., Gaina, C., 2008. Global plate motion frames: Toward a unified model. Reviews of Geophysics 46. doi:10.1029/2007RG000227.

Turcotte, D.L., Schubert, G., 1982. Geodynamics. John Wiley and Sons, New York. pp. 134–159.

Čadek, O., Fleitout, L., 2003. Effect of lateral viscosity variations in the top 300 km on the geoid and dynamic topography. Geophys. J. Int. 152, 566–580. doi:10.1046/j.1365-246X.2003.01859.x.

Čadek, O., Ricard, Y., 1992. Toroidal poloidal energy partitioning and global lithospheric rotation during cenozoic time. Earth Planet. Sci. Lett. 109, 621–632. doi:10.1016/0012-821X(92)90120-K.

Čížková, H., van den Berg, A.P., Spakman, W., Matyska, C., 2012. The viscosity of earth's lower mantle inferred from sinking speed of subducted lithosphere. Phys. Earth Planet. Inter. 200, 56–62. doi:10.1016/j.pepi.2012.02.010.

738 Čížková, H., Bina, C., 2013. Effects of mantle and subduction-interface
739 rheologies on slab stagnation and trench rollback. Earth Planet. Sci. Lett.
740 , 95–103doi:10.1016/j.epsl.2013.08.011.
741 Čížková, H., Bina, C., 2019. Linked influences on slab stagnation: Interplay
742 between lower mantle viscosity structure, phase transitions, and plate
743 coupling. Earth Planet. Sci. Lett. , 88–99doi:10.1016/j.epsl.2018.12.
744 027.
745 Walpole, J., Wookey, J., Kendall, J.M., Masters, T.G., 2017. Seis-
746 mic anisotropy and mantle flow below subducting slabs. Earth
747 Planet. Sci. Lett. 465, 155–167. doi:10.1016/j.epsl.2017.02.023.
748 Yang, T., Gurnis, M., 2016. Dynamic topography, gravity and the role
749 of lateral viscosity variations from inversion of global mantle flow.
750 Geophys. J. Int. 207, 1186–1202. doi:10.1093/gji/ggw335.
751 Yang, T., Moresi, L., Zhao, D., Sandiford, D., Whittaker, J., 2018. Cenozoic
752 lithospheric deformation in northeast asia and the rapidly-aging pacific
753 plate. Earth Planet. Sci. Lett. doi:10.1016/j.epsl.2018.03.057.